

OMICS Journals are welcoming Submissions

OMICS International welcomes submissions that are original and technically so as to serve both the developing world and developed countries in the best possible way.

OMICS Journals are poised in excellence by publishing high quality research. OMICS International follows an Editorial Manager® System peer review process and boasts of a strong and active editorial board.

Editors and reviewers are experts in their field and provide anonymous, unbiased and detailed reviews of all submissions. The journal gives the options of multiple language translations for all the articles and all archived articles are available in HTML, XML, PDF and audio formats. Also, all the published articles are archived in repositories and indexing services like DOAJ, CAS, Google Scholar, Scientific Commons, Index Copernicus, EBSCO, HINARI and GALE.

For more details please visit our website:

<http://omicsonline.org/Submitmanuscript.php>

Understanding of workpiece defects induced by laser beam

P. S. Wei

Xi-Wan Chair Professor

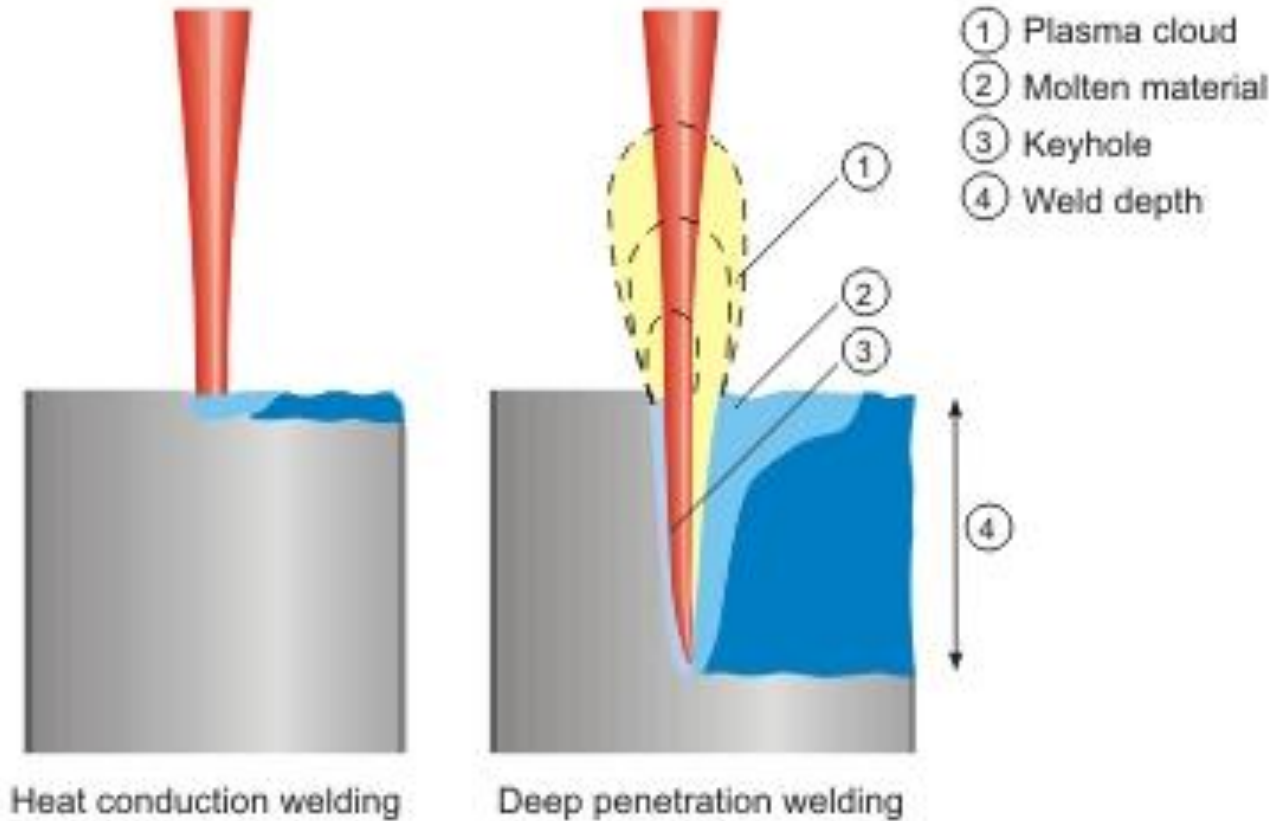
Department of Mechanical and Electro-Mechanical Engineering

National Sun Yat-Sen University

Kaohsiung, Taiwan 80424, ROC

E-mail: pswei@mail.nsysu.edu.tw

This presentation deals with (1) defects of surface rippling and humping and root spiking and (2) pore formation due to super-saturation and liquid entrapment after solidification. Surface rippling and humping often accompany solute segregation, porosity, crack, deformation, etc. Spiking accompanies cold shut and porosity is another severe defect. Incapable drilling also results from collapse of the induced keyhole. Finding mechanisms of these defects is essentially required to control qualities of workpieces.



Laser welding or melting

(http://www.rofin.com/en/applications/laser_welding/welding_methods/)

Experimental setup

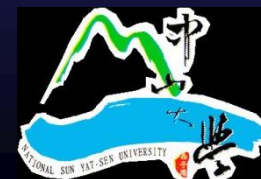
NSYSU

Mechanical & Micro-Mechanical
Engineering



TORVAC EBW, max. 60 kV, 50 mA, 60 mm/s, 3000 W

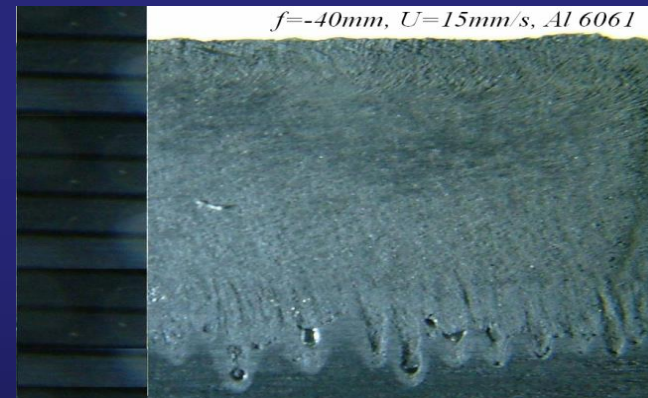
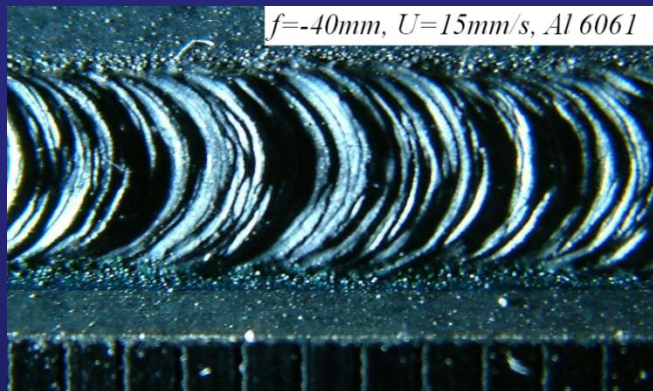
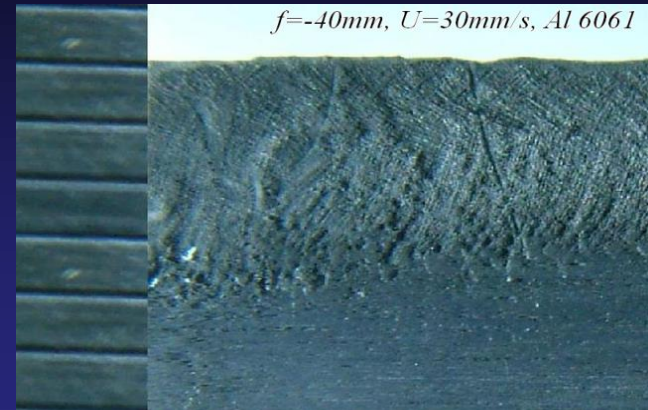
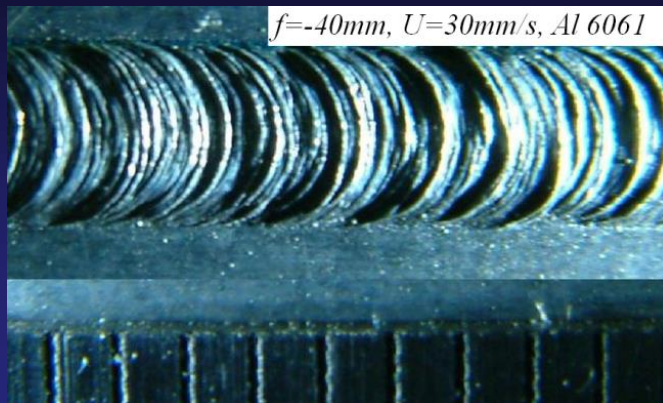
Heat Transfer Lab for Manufacturing and Materials Processing



Observation and measurements

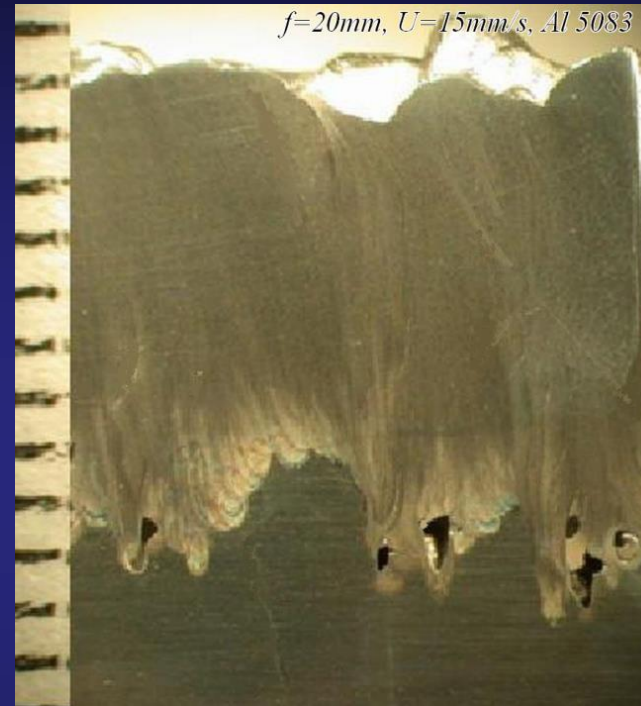
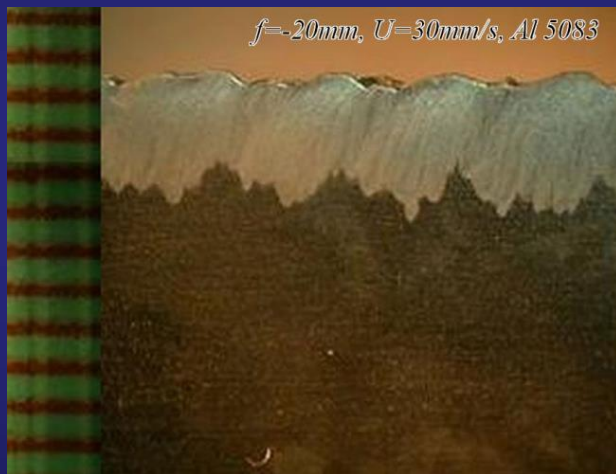
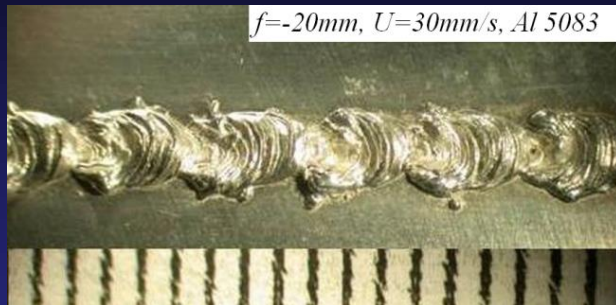
NSYSU

Mechanical & Micro-Mechanical
Engineering



Rippling and spiking are decreased by increasing welding speed. Porosity can also be seen near the spiking tip (Wei et al. 2012, IEEE Trans. CPMT)

(continued)



Spiking and humping are decreased by increasing welding speed and raising focal location. Porosity can also be seen near the spiking tip (Wei et al. 2012. IEEE Trans. CPMT)

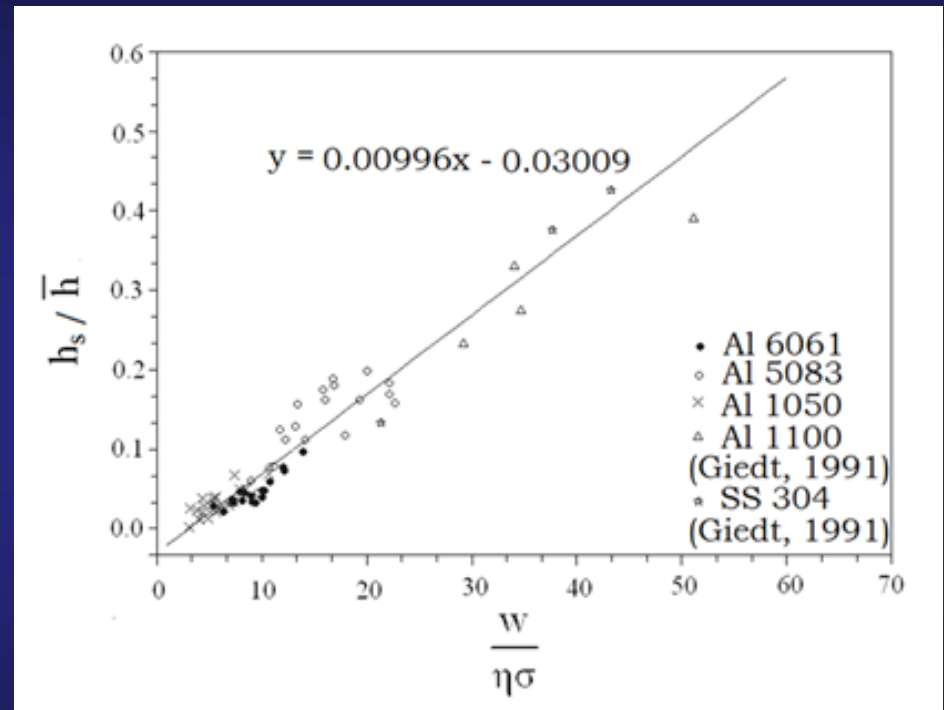
(continued)

Spiking tendency by considering energy conservation in welding and vertical directions is given by (Wei et al. 2012, IEEE Trans. CPMT)

$$\frac{h_s}{\bar{h}} \sim \frac{w}{\eta\sigma}$$

where melting efficiency is

$$\eta = \frac{1}{1 + c_2 \sqrt{1 + \left(\frac{w}{2\bar{h}}\right)^2 \left(\frac{1}{Pe} + c_1\right) \frac{Ste}{Ste + 1}}}$$



In above equations, h_s , \bar{h} , w , and σ are spiking amplitude, average fusion zone depth and width, and beam radius. Pe and Ste are the Peclet and Stefan numbers, c_1 and c_2 empirical constants, respectively.

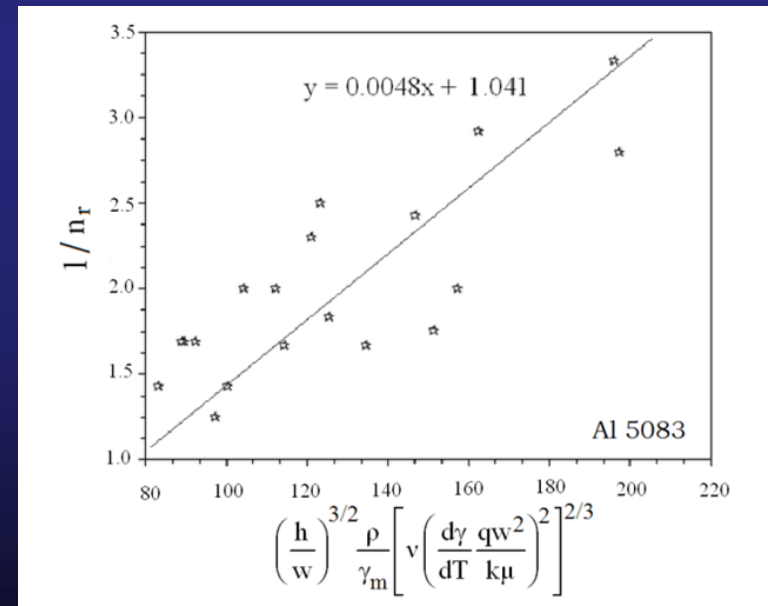
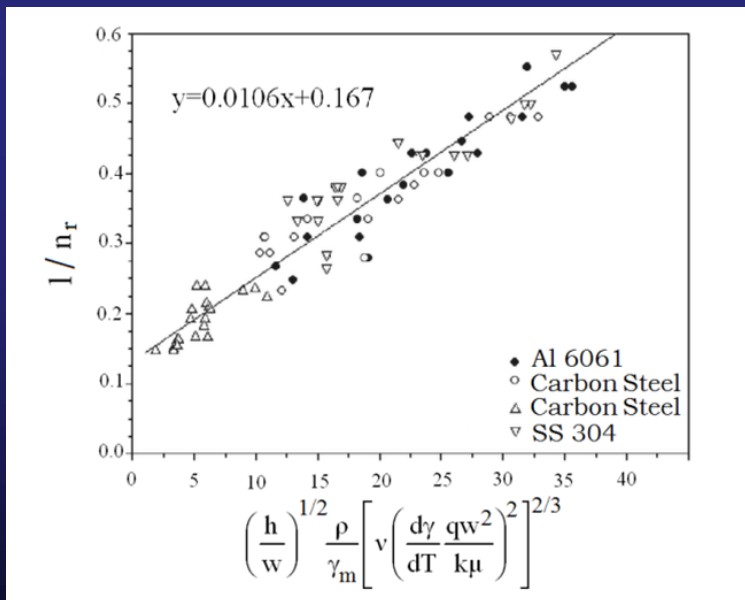
(continued)

Average pitch of humping or spiking for alloys in the absence and presence of volatile elements are, respectively,

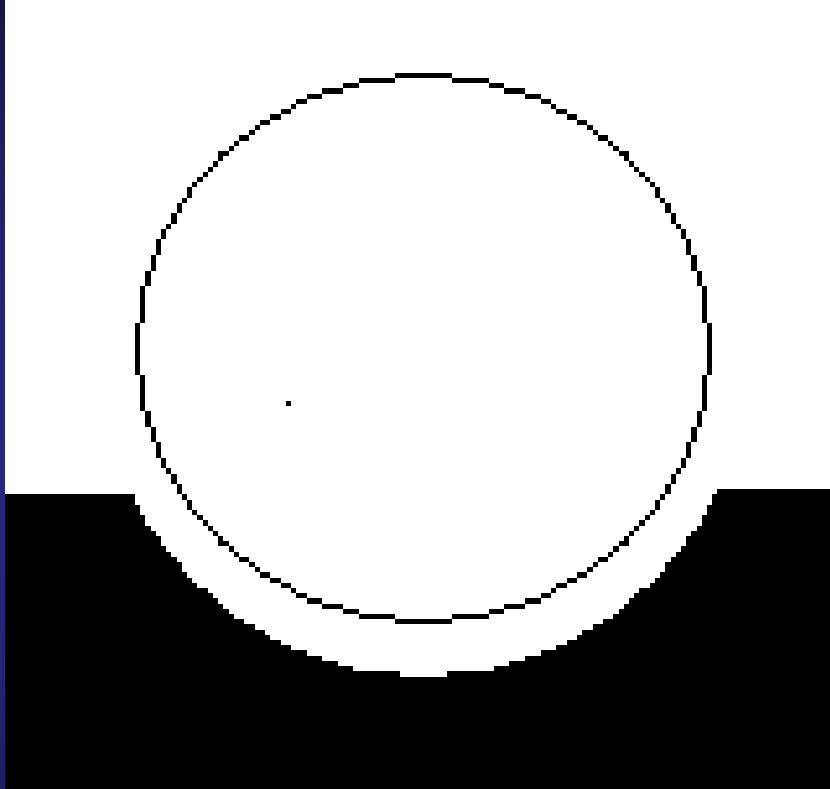
$$\frac{1}{n_r} \sim \left(\frac{\bar{h}}{w}\right)^{1/2} \frac{\rho}{\gamma_m} \left[\nu \left(\frac{d\gamma}{dT} \frac{qw^2}{\mu k_\ell} \right)^2 \right]^{2/3}$$

$$\frac{1}{n_r} \sim \left(\frac{\bar{h}}{w}\right)^{3/2} \frac{\rho}{\gamma_m} \left[\nu \left(\frac{d\gamma}{dT} \frac{qw^2}{\mu k_\ell} \right)^2 \right]^{2/3}$$

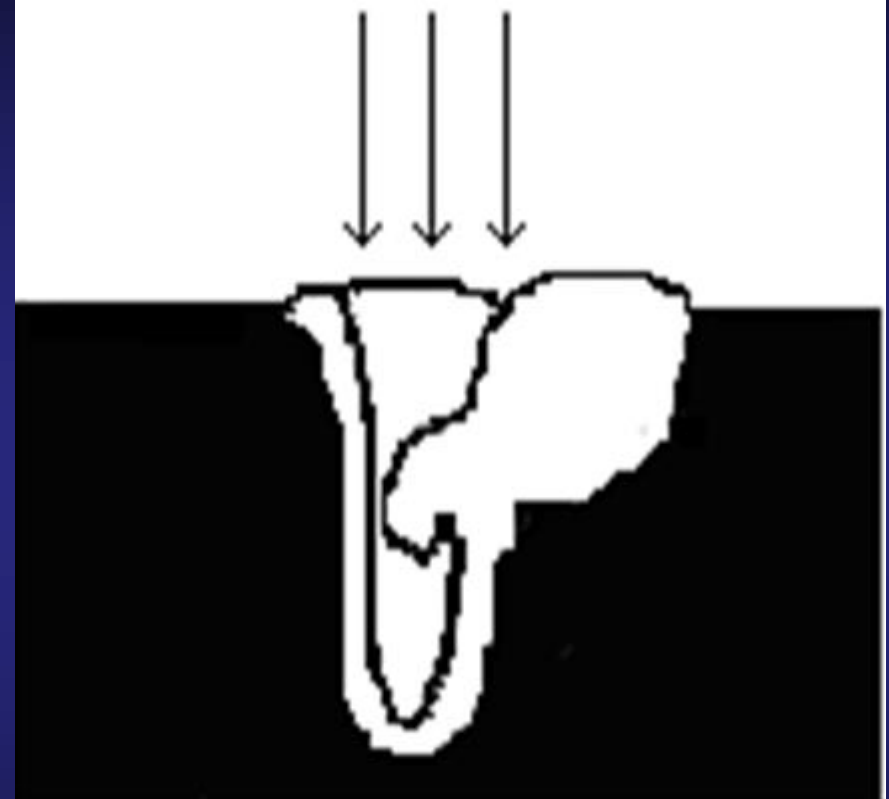
where $\rho, \gamma_m, \nu, \mu, d\gamma/dT, q$, and k_ℓ are density, surface tension, kinematic and dynamic viscosities, surface tension coefficient, incident flux and liquid thermal conductivity, respectively.



Pore formation

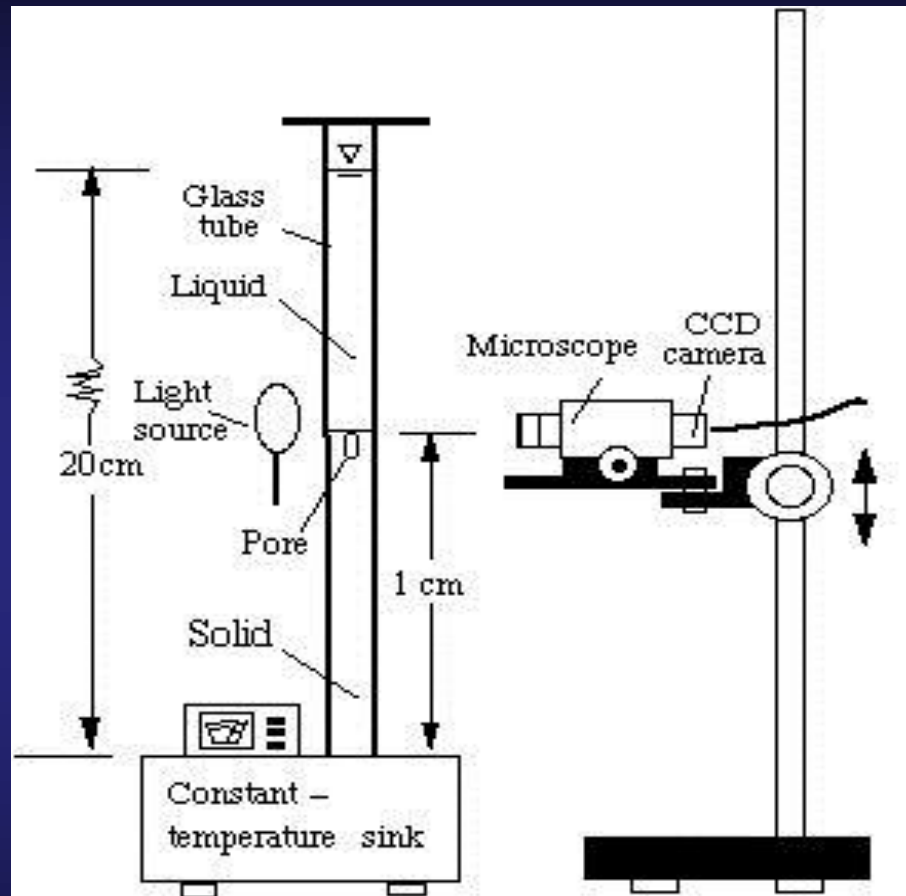


Bubble nucleated due to super-saturation



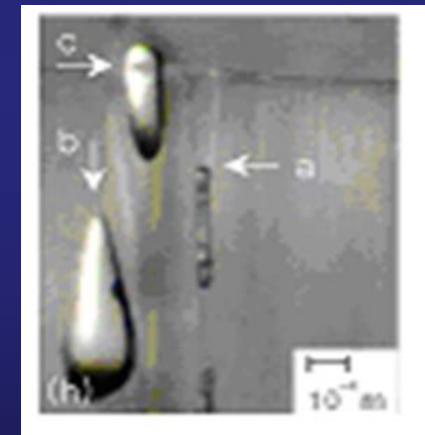
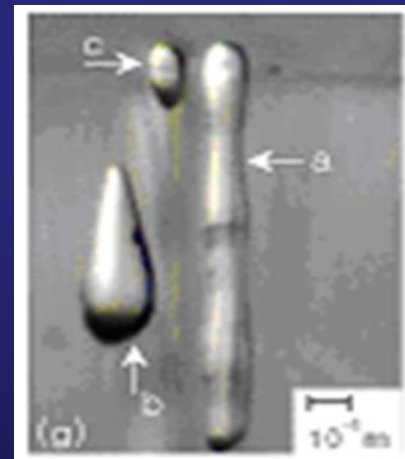
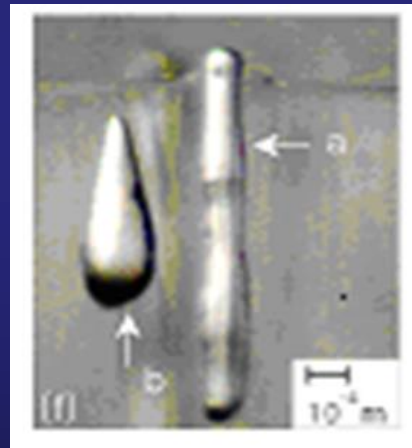
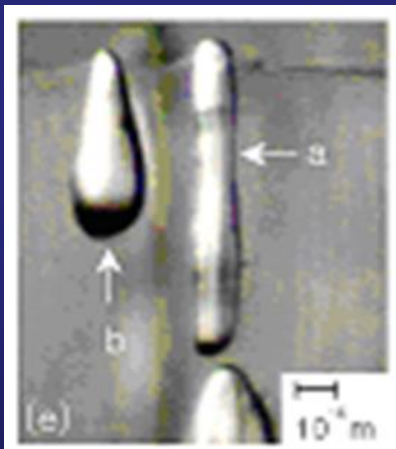
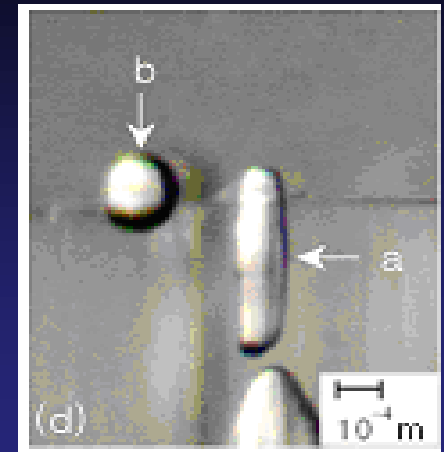
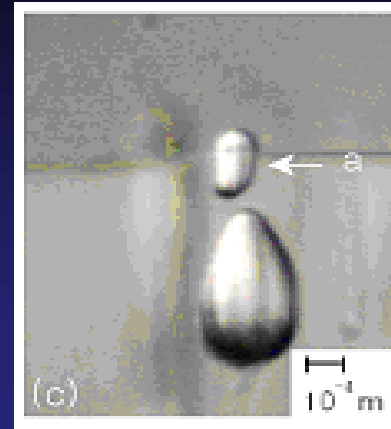
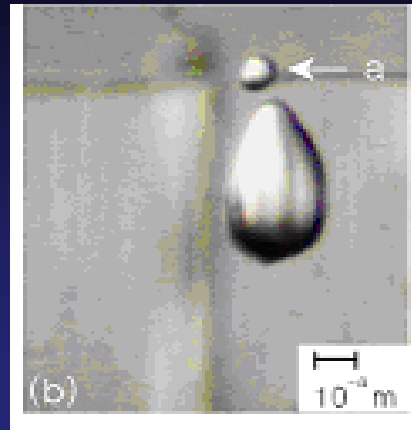
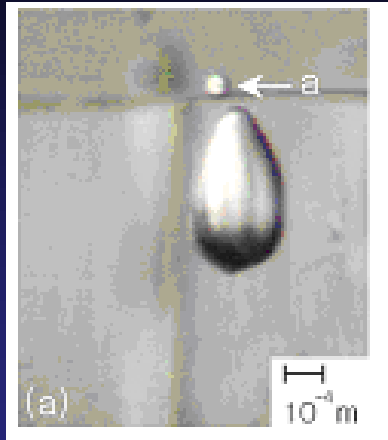
Pore formation due to liquid entrapment in keyhole welding
(Pastor et al. 2001, Weld. Int.)

Experimental setup



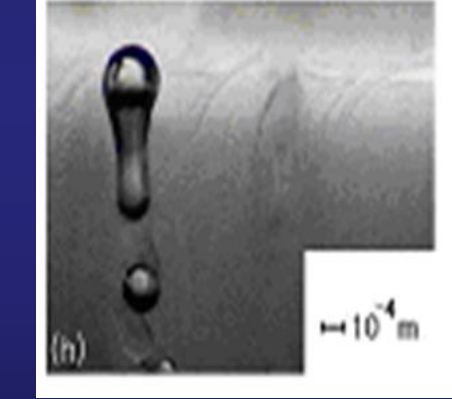
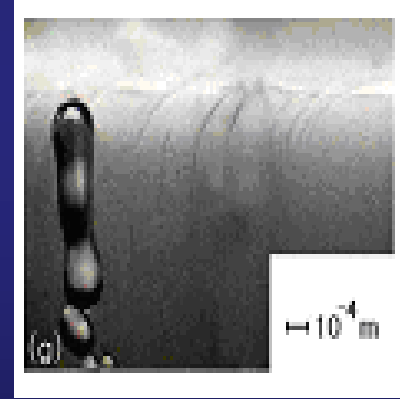
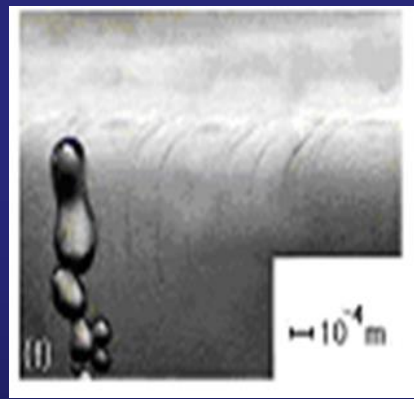
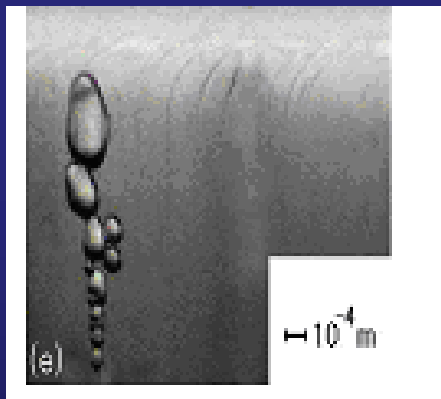
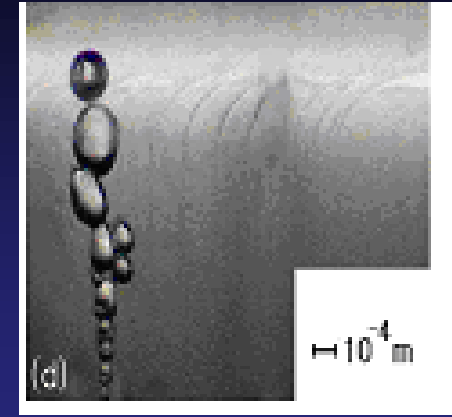
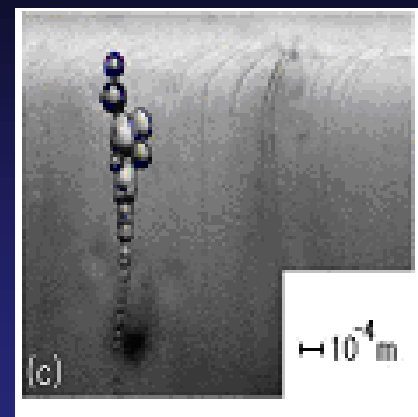
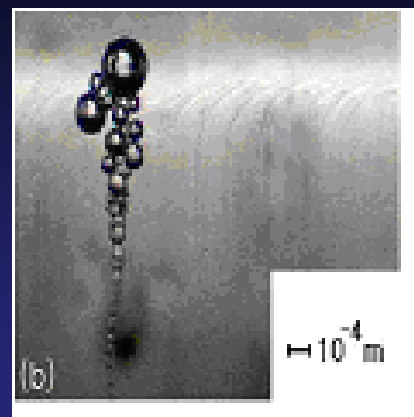
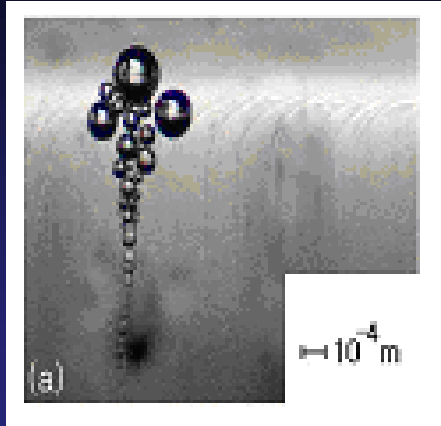
Experimental Setup (Wei et al. 2003, Metall. Mater. Trans B;
Wei et al. 2004, JCG)

(continued)



Bubbles trapped in solid at different times or locations near the location of 1 cm (a) 0, (b) 5, (c) 20, (d) 60, (e) 120, (f) 150, (g) 180, and (h) 206 s during the freezing of water containing oxygen gas content of 0.0041 g/100 g and temperature of the constant temperature sink of -25°C (Wei et al. 2004, JCG).

(continued)



Bubbles trapped in solid at different times or locations near a location of 1 cm
(a) 0 s, (b) 450 s, (c) 540 s, (d) 810 s, (e) 900 s, (f) 1170 s, (g) 1350 s, (h) 1440 s
during the freezing of water containing oxygen gas content of 0.0037 g/100 g
and temperature of -25°C of the constant temperature sink (Wei et al. 2004).

Pore formation due to super-saturation

Differentiating equation of state with time

$$\frac{dp_g}{dt} V + p_g \frac{dV}{dt} = \frac{dn_g}{dt} RT$$

Mass transfer to the bubble is given by

$$\frac{dn_g}{dt} = h_D \pi r_B^2 (C_\infty - C_{\ell,w})$$

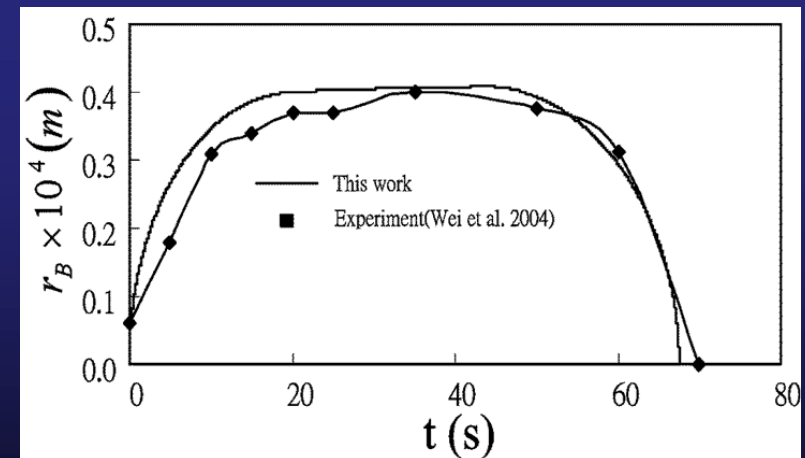
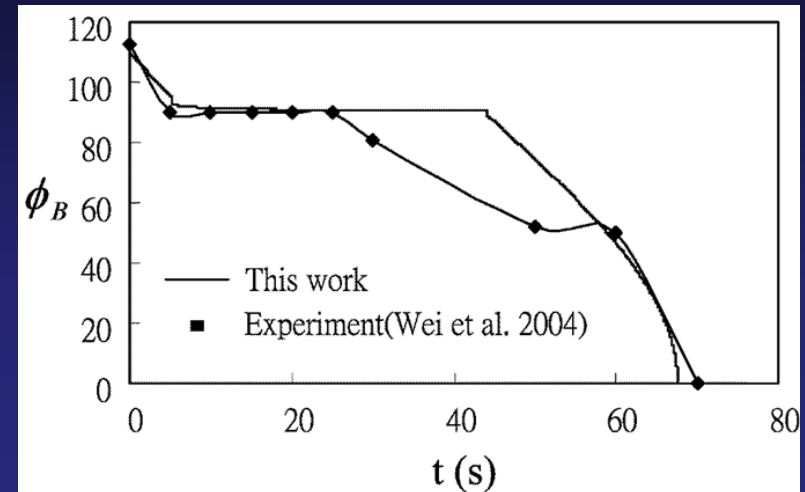
Volume change rate is

$$\frac{dV}{dt} = \pi r_B^2 \frac{ds}{dt}$$

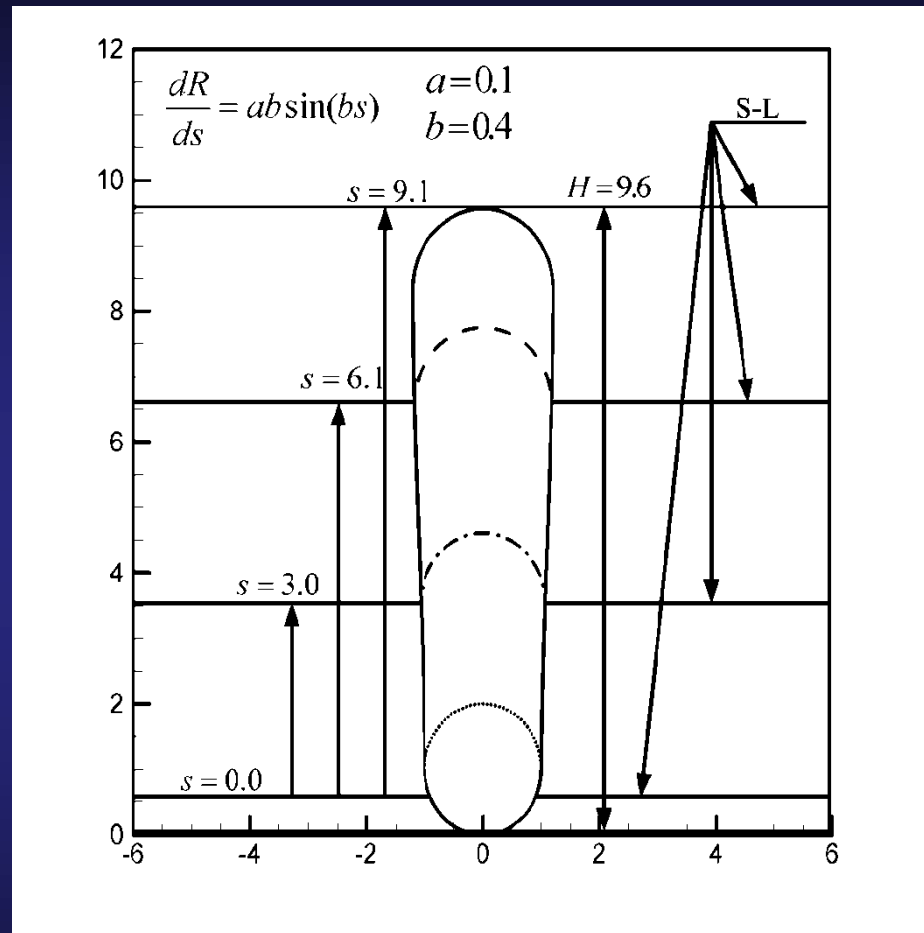
Henry's law is

$$p_g = KC_{\ell,w}$$

where p_g , V , n_g , T , and R are, respectively, pressure, volume, mole of gas and temperature in the pore, and specific gas constant, h_D , r_B , $C_{\ell,w}$, C_∞ , s , and K the mass transfer coefficient, pore radius, concentration at the bubble cap and infinity, solification front displacement and Henry constant.



(continued)



Development of pore shape for $dR/ds = 0.04\sin(0.4s)$ (Wei and Hsiao, 2012)

(continued)

Equations of mass, momentum are, respectively

$$\frac{\partial \rho}{\partial t} + \left(u \frac{\partial \rho}{\partial x} + v \frac{\partial \rho}{\partial y} \right) + \rho \left(\frac{\partial u}{\partial x} + \frac{\partial v}{\partial y} \right) = 0$$

$$\rho \frac{Du}{Dt} = -\frac{\partial P}{\partial x} + 2 \frac{\partial}{\partial x} \left(\mu \frac{\partial u}{\partial x} \right) + \frac{\partial}{\partial y} \left[\mu \left(\frac{\partial v}{\partial x} + \frac{\partial u}{\partial y} \right) \right] - \frac{2}{3} \frac{\partial}{\partial x} \left[\mu \left(\frac{\partial u}{\partial x} + \frac{\partial v}{\partial y} \right) \right]$$

$$+ \left[-\gamma \kappa \mathbf{n} - \frac{d\gamma}{dT} (\nabla T - (\mathbf{n} \cdot \nabla T) \mathbf{n}) - \frac{d\gamma}{dC} (\nabla C - (\mathbf{n} \cdot \nabla C) \mathbf{n}) \right] \cdot \mathbf{i} \delta (n - n_s)$$

$$\rho \frac{Dv}{Dt} = -\frac{\partial P}{\partial y} + 2 \frac{\partial}{\partial y} \left(\mu \frac{\partial v}{\partial y} \right) + \frac{\partial}{\partial x} \left[\mu \left(\frac{\partial v}{\partial x} + \frac{\partial u}{\partial y} \right) \right] - \frac{2}{3} \frac{\partial}{\partial y} \left[\mu \left(\frac{\partial u}{\partial x} + \frac{\partial v}{\partial y} \right) \right] + \rho g$$

$$+ \left[-\gamma \kappa \mathbf{n} - \frac{d\gamma}{dT} (\nabla T - (\mathbf{n} \cdot \nabla T) \mathbf{n}) - \frac{d\gamma}{dC} (\nabla C - (\mathbf{n} \cdot \nabla C) \mathbf{n}) \right] \cdot \mathbf{j} \delta (n - n_s)$$

(continued)

Conservation equations of energy, concentration and phase field equations are, respectively

$$\frac{\partial(\rho h)}{\partial t} + \frac{\partial(\rho u h)}{\partial x} + \frac{\partial(\rho v h)}{\partial y} = \frac{\partial}{\partial x} \left(k \frac{\partial T}{\partial x} \right) + \frac{\partial}{\partial y} \left(k \frac{\partial T}{\partial y} \right) - \left[\frac{\partial}{\partial t} (\rho L) + \frac{\partial}{\partial x} (\rho u L) + \frac{\partial}{\partial y} (\rho v L) \right]$$

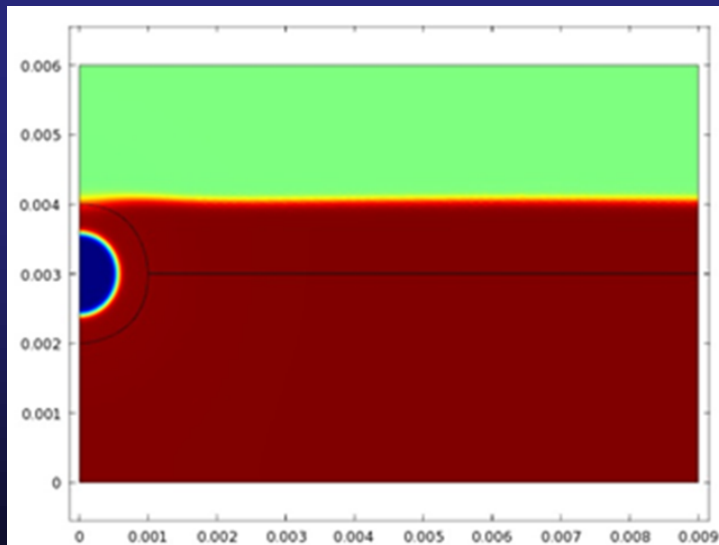
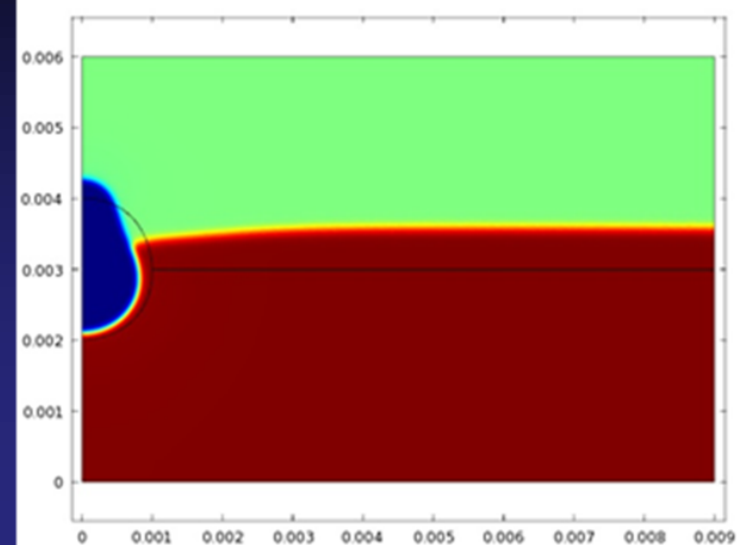
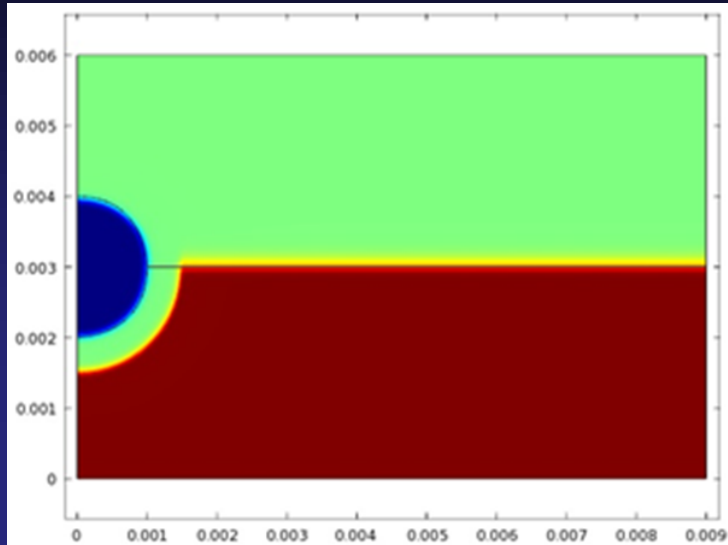
$$\frac{\partial C}{\partial t} + \frac{\partial(uC)}{\partial x} + \frac{\partial(vh)}{\partial y} = \frac{\partial}{\partial x} \left(D \frac{\partial C}{\partial x} \right) + \frac{\partial}{\partial y} \left(D \frac{\partial C}{\partial y} \right) - \left[\frac{\partial}{\partial t} (C) + \frac{\partial}{\partial x} (uC) + \frac{\partial}{\partial y} (vC) \right]$$

$$\frac{\partial \phi}{\partial t} + \mathbf{v} \cdot \nabla \phi = \gamma_L \lambda \nabla^2 \left[-\nabla^2 \phi + \frac{\phi(\phi^2 - 1)}{\epsilon_{pf}} \right]$$

where surface curvature $\kappa = \nabla \cdot \mathbf{n} = \frac{1}{\|\nabla \phi\|} \left[\nabla^2 \phi - \frac{(\nabla \phi \cdot \nabla) \|\nabla \phi\|}{\|\nabla \phi\|} \right],$

Delta function $\delta(\mathbf{n} - \mathbf{n}_s) = 3(1 - \phi^2) |\nabla \phi| / 4$

(continued)



Predict pore formation in aluminum

Pore formation due to liquid entrapment

Equations of mass, momentum and energy are, respectively

$$\frac{d\tilde{\rho}_c}{\tilde{\rho}_c} + \frac{d\tilde{u}_c}{\tilde{u}_c} + \frac{d\tilde{A}_c}{\tilde{A}_c} = \frac{d\tilde{W}_c}{\tilde{W}_c}$$

$$\tilde{\rho}_c \tilde{u}_c d\tilde{u}_c + \tilde{\rho}_c g d\tilde{Z} + d\tilde{p}_c + \frac{4\tilde{\tau}_{im} d\tilde{s}}{\tilde{D}_h} + \tilde{\rho}_c \tilde{u}_c^2 (1 - \phi) \frac{d\tilde{W}_c}{\tilde{W}_c} = 0$$

$$d\tilde{q} = d\tilde{h}_c + d\frac{\tilde{u}_c^2}{2} + (\tilde{H}_c - \tilde{H}_E) \frac{d\tilde{W}_i}{\tilde{W}_i}$$

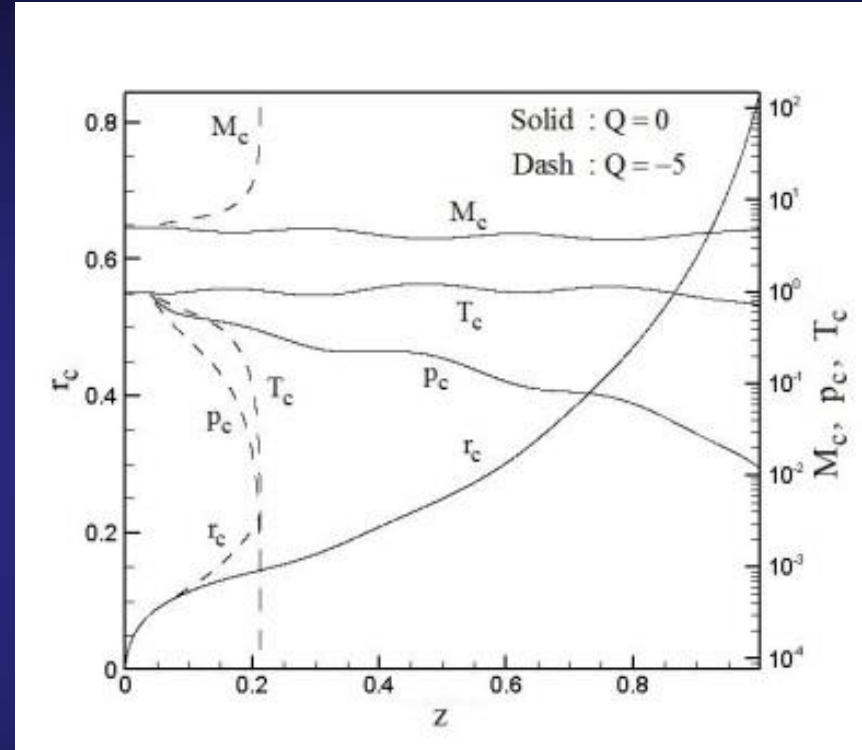
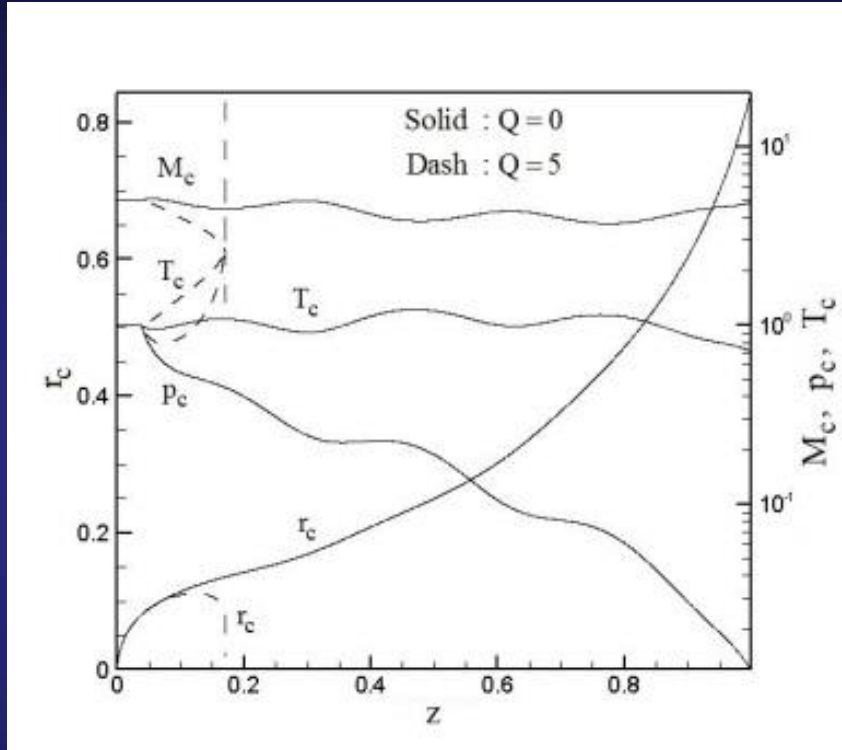
Consider Young-Laplace equation

$$p_c + \frac{j_E^2}{\rho_c} = p_\ell + \Gamma \left(\frac{1}{R_1} + \frac{1}{R_2} \right)$$

where $\tilde{\tau}_{im}$, \tilde{D}_h , ϕ , and \tilde{W}_c are shear stress, hydraulic diameter, axial velocity component ratio between entrainment and mixture through the core region, and mass rate through the keyhole, \tilde{q} , \tilde{h}_c , \tilde{H}_E , \tilde{H}_c , \tilde{j}_E , R_1 , R_2 and Γ the absorbed energy, total energy of entrainment and mixture gas, entrainment flux, radii of principle curvatures, and surface tension paramter.

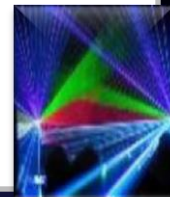
- The higher the gas pressure, the easier and smaller the pore can be formed

(continued)



Pore formation or keyhole collapse for energy absorption for a supersonic flow
(Wei et al. 2014, IEEE Trans. CPMT)

- Mechanisms of different types of surface patterns such as rippling, gouging, undercut, and humping, and root spiking are still unclear.
- Pore formation is characterized by different mechanisms: (1) supersaturation of dissolved gases in liquid ahead of the solidification front, and (2) liquid entrapment such as keyhole collapse during keyhole welding.
- All these defects involve strong deformation of the free surface and different types of instabilities coupled with complicated transport processes. Controlling factors need to be clarified and determined.



- Journal of Photonics
- Journal of Wave theory
- Journal of Optics
- Journal of Lasers
- Signal Crystal





For upcoming Conference visit
<http://www.conferenceseries.com/>

